DSE/2538-2

DEVELOPMENT OF A THIN FILM POLYCRYSTALLINE SOLAR CELL FOR LARGE SCALE TERRESTRIAL USE

Quarterly Progress Report, October 1—December 31, 1976

May 1977

Work Performed Under Contract No. EX-76-C-01-2538

University of Delaware
Institute of Energy Conversion
Newark, Delaware

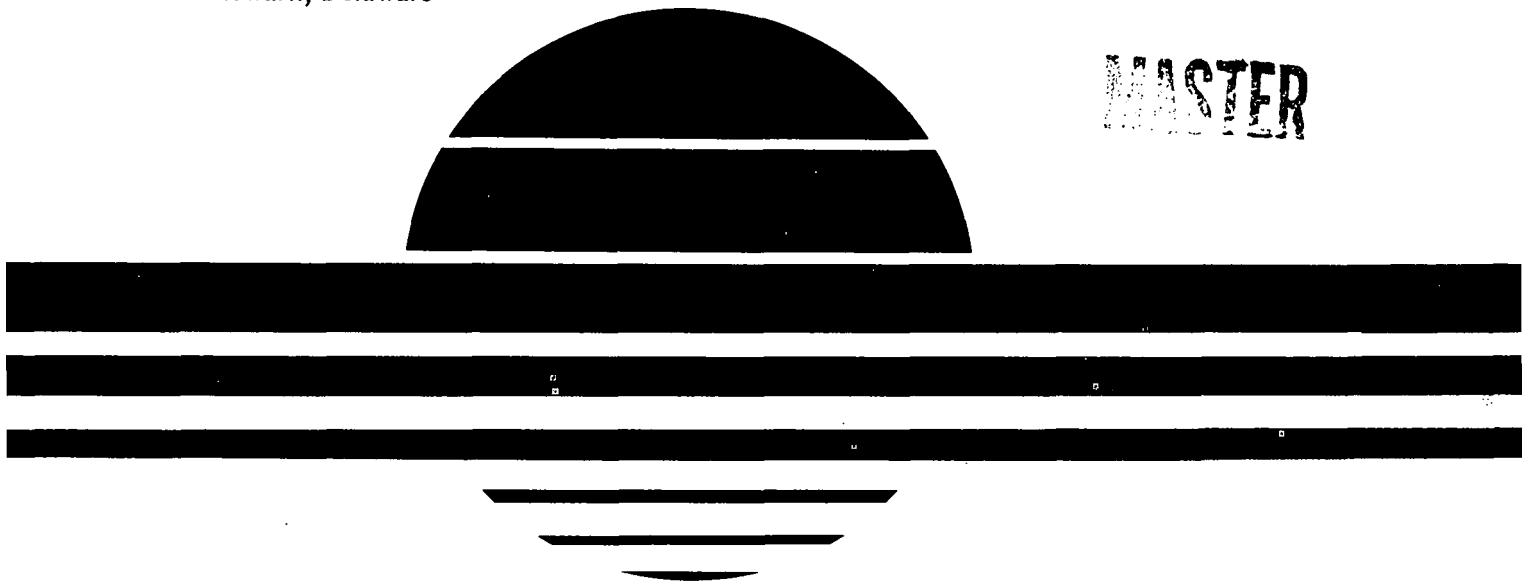

U.S. Department of Energy

Solar Energy

NOTICE

DSE/2538-2
Distribution Category UC-63e

DEVELOPMENT OF A THIN FILM POLYCRYSTALLINE SOLAR CELL FOR LARGE SCALE TERRESTRIAL USE

Quarterly Progress Report

October 1, 1976 - December 31, 1976

E(49-18)-2538

May 1977

INSTITUTE OF ENERGY CONVERSION

UNIVERSITY OF DELAWARE

NEWARK, DELAWARE 19711

Supported by the Energy Research and Development Administration

BIBLIOGRAPHIC DATA SHEET	1. Report No. E(49-18)-2538	2.	3. Recipient's Accession No.
4. Title and Subtitle Development of a Thin Film Polycrystalline Solar Cell for Large Scale Terrestrial Use			5. Report Date May 1, 1977 6.
7. Author(s)			8. Performing Organization Rept. No.
9. Performing Organization Name and Address Institute of Energy Conversion University of Delaware Newark, Delaware 19711			10. Project/Task/Work Unit No. 11. Contract/Grant No. E(49-18)-2538
12. Sponsoring Organization Name and Address Division of Solar Energy Energy Research and Development Administration 20 Massachusetts Avenue, N. W. Washington, DC 20545			13. Type of Report & Period Covered 10/1/76 - 12/31/76 14.
15. Supplementary Notes			

16. Abstracts

The maximum short circuit current for CdS/Cu_2S cell has now been increased to 21.9 mA/cm^2. During the coming quarter, application of the redesigned grid structure is expected to yield CdS/Cu_2S cells with over 8% conversion efficiency.

The short circuit currents achieved with the $(CdZn)S/Cu_2S$ cells are showing marked improvement. Currents in excess of 12 mA/cm^2 have been achieved at open circuit voltages of 0.67 V and over 10 mA/cm^2 at open circuit voltages of 0.60 V.

Direct experimental observations coupled with theoretical analyses have been conducted on the influence of the Cu_2S sheet resistivity on cell performance. Further refinements have been made in the theoretical analysis of fill factor. Spectral response and photocapacitance measurements have been made on the mixed sulfide cells.

17. Key Words and Document Analysis. 17a. Descriptors

Photovoltaic Conversion

CdS Solar Cells

Heterojunctions

17b. Identifiers/Open-Ended Terms

Solar Energy

17c. COSATI Field/Group

18. Availability Statement	19. Security Class (This Report) UNCLASSIFIED	21. No. of Pages
	20. Security Class (This Page UNCLASSIFIED	22. Price

FORM NTIS-35 (REV. 3-72)

USCOMM-DC 14952-P72

Abstract

The maximum short circuit current for CdS/Cu_2S cell has now been increased to 21.9 mA/cm^2. During the coming quarter, application of the redesigned grid structure is expected to yield CdS/Cu_2S cells with over 8% conversion efficiency.

The short circuit currents achieved with the $(CdZn)S/Cu_2S$ cells are showing marked improvement. Currents in excess of 12 mA/cm^2 have been achieved at open circuit voltages of 0.67 V and over 10 mA/cm^2 at open circuit voltages of 0.60 V.

Direct experimental observations coupled with theoretical analyses have been conducted on the influence of the Cu_2S sheet resistivity on cell performance. Further refinements have been made in the theoretical analysis of fill factor. Spectral response and photocapacitance measurements have been made on the mixed sulfide cells.

2nd Quarterly, October 1, 1976 - December 31, 1976

2. Table of Contents

	Page
Bibliographic Data Sheet	ii
1. Abstract	1
2. Table of Contents	3
List of Illustrations	4
List of Tables	5
3. Summary	6
4. Introduction	8
4.1 Objectives	8
4.2 Approach and Key Methods	8
5. Cell Production and Analysis	9
5.1 Development of High Efficiency CdS/Cu_2S Cells	9
5.2 Development of (CdZn)S/Cu_2S Cells	19
5.3 Cu_2S Films	25
5.4 Electro-Optical Analysis	26
5.5 Theoretical Analysis	43
6. References	53
APPENDIX A. List of Research Contributors	54

Figures

Figure 1. Cell design for an all evaporated grid structure.

Figure 2. Distribution of CdS resistivity.

Figure 3. Variation of CdS resistivity on a 8 x 8 cm substrate.

Figure 4. Variation of open circuit voltage with zinc content.

Figure 5. Variation of short circuit current with zinc content.

Figure 6. Influence of heat treatment on open circuit voltage and short circuit current for (CdZn)S/Cu_2S cells.

Figure 7. Contact configuration for van der Pauw technique.

Figure 8. Influence of temperature on the sheet resistance of Cu_2S on cell 378-1.

Figure 9. Open circuit voltage decay with time for (CdZn)S/Cu_2S cell 378-1.

Figure 10. Space charge profiles in the CdS/Cu_2S junction.

Figure 11. Energy band diagram for the CdS/Cu_2S junction.

Tables

Table 1. W-I simulated and actual sunlight tests for cell #312-4A.

Table 2. The influence of etching on cell performance.

Table 3. Cell variation from a single CdS substrate.

Table 4. Cell parameters for dry process unetched CdS/Cu_2S cells.

Table 5. Cell parameters for dry process etched CdS/Cu_2S cells.

Table 6. Comparison between cells produced by solution and solid state reaction.

Table 7. Comparison between NASA-Lewis and I.E.C. test results on (CdZn)S/Cu_2S cells.

Table 8. Sheet resistance of Cu_2S after various treatments.

Table 9. Development of sheet resistance for Cu_2S on (CdZn)S substrates.

Table 10. Fill factor for various grid geometries.

Table 11. Spectral response peaks for CdS and (CdZn)S cells.

3. Summary

The maximum short circuit current for a CdS/Cu_2S cell has been increased to 21.9 mA/cm^2. As improvements are made in fill factor, this current will correspond to coversion efficiencies close to 8.0%.

The (CdZn)S/Cu_2S cell conversion efficiency has previously been dominated by the low short circuit currents achieved. During this quarter, substantial improvements have been made in currents resulting in values in excess of 12 mA/cm^2 at open circuit voltages of 0.67 V and in excess of 10 mA/cm^2 at open circuit voltages of 0.60 V. These results were verified by testing at NASA-Lewis.

Work has continued in the production of Cu_2S films by direct reaction with a copper substrate. The films produced to date have had defects in them which has prevented the production of Schottky diodes with evaporated metal contacts. Alternate techniques of producing Cu_2S films will be explored during the coming quarter.

The close coupling between analysis and cell production has continued. This quarter van der Pauw techniques have been used to monitor the sheet resistance in the Cu_2S layer of a cell during various stages of production. These observations have been coupled with a thorough analysis of the influence of resistive components and other parameters on fill factor. The spectral response for the mixed sulfide cells has been measured and the results related to observations on photo-capacitance.

Further refinements have been made in a theoretical modeling of the influence of Cu_2S stoichiometry on overall cell performance. In

addition, more detailed studies have been made of the space charge region and these analyses related to cell performance.

4. Introduction

This program is aimed at developing a thin film polycrystalline cell of over 10% conversion efficiency. Two heterojunctions are being developed - CdS/Cu_2S and (CdZn)S/Cu_2S.

4.1 Objectives

The overriding objective of the present program is to produce a thin film polycrystalline cell with an energy converison efficiency in direct sunlight of at least 10%.

To reach the above objective as expeditiously as possible, improved and expanded materials and electronic analytical capabilities will be developed.

4.2 Approach and Key Methods

The basic cell production technique will continue to be vapor deposition. Techniques have been established for the production of controlled CdS and (CdZn)S layers. The surface layer of Cu_2S is being produced by both solution and solid state reaction techniques.

All cell production will be directed by ongoing modeling and analysis. In response to this approach, the CdS/Cu_2S cell efficiency has been raised close to 8% and marked improvements in (CdZn)S cell currents have been achieved.

5.1 Development of High Efficiency CdS/Cu_2S Cells

At the end of the last quarter, it was reported that the 40 ℓpi grids were limiting ultimate cell efficiency. The major cause was the Cu_2S sheet resistance increase as reducing heat treatments raised the Cu_2S stoichiometry. A full analysis of the situation is presented in Section 5.4.

Analysis of the optimum grid configuration shows that a spacing in the region of 60 to 80 ℓpi is necessary at the current levels being achieved and masks for these two spacings, are on order. To maintain 96% transmissivity line widths of 0.0005" (12.5 μm) have been specified, this representing about the limit with vapor deposition techniques. To avoid significant losses due to grid line resistance, an increase in Au thickness to > 1.5 μm is necessary. This is not achievable with a resistance heated source and accordingly a 5 kWatt electron beam source has been brought on line. Actual line thicknesses are now ∿ 2.5 μm to avoid line breakage at the step onto the gold collection tab. Figure 1 shows the final cell design; the insulated tab was described in the previous report.[1]

The highest efficiencies achieved to date (7.77%) were with the hybrid grid structure developed during June 1976. The cell design to give substantial improvement involves an all-evaporated grid with a more effective A-R coating than the cover plastic integral to the hybrid grid design. Progress with this cell design continues but major advance is dependent on application of the 60 or 80 ℓpi grid. Tests with SiO A-R coatings consistently shows current enhancement of ∿ 7% and the highest J_{sc} to date 21.9 mA/cm^2 has been achieved with this coating. Table 1 gives the best cell results for an all-evaporated grid structure with the current

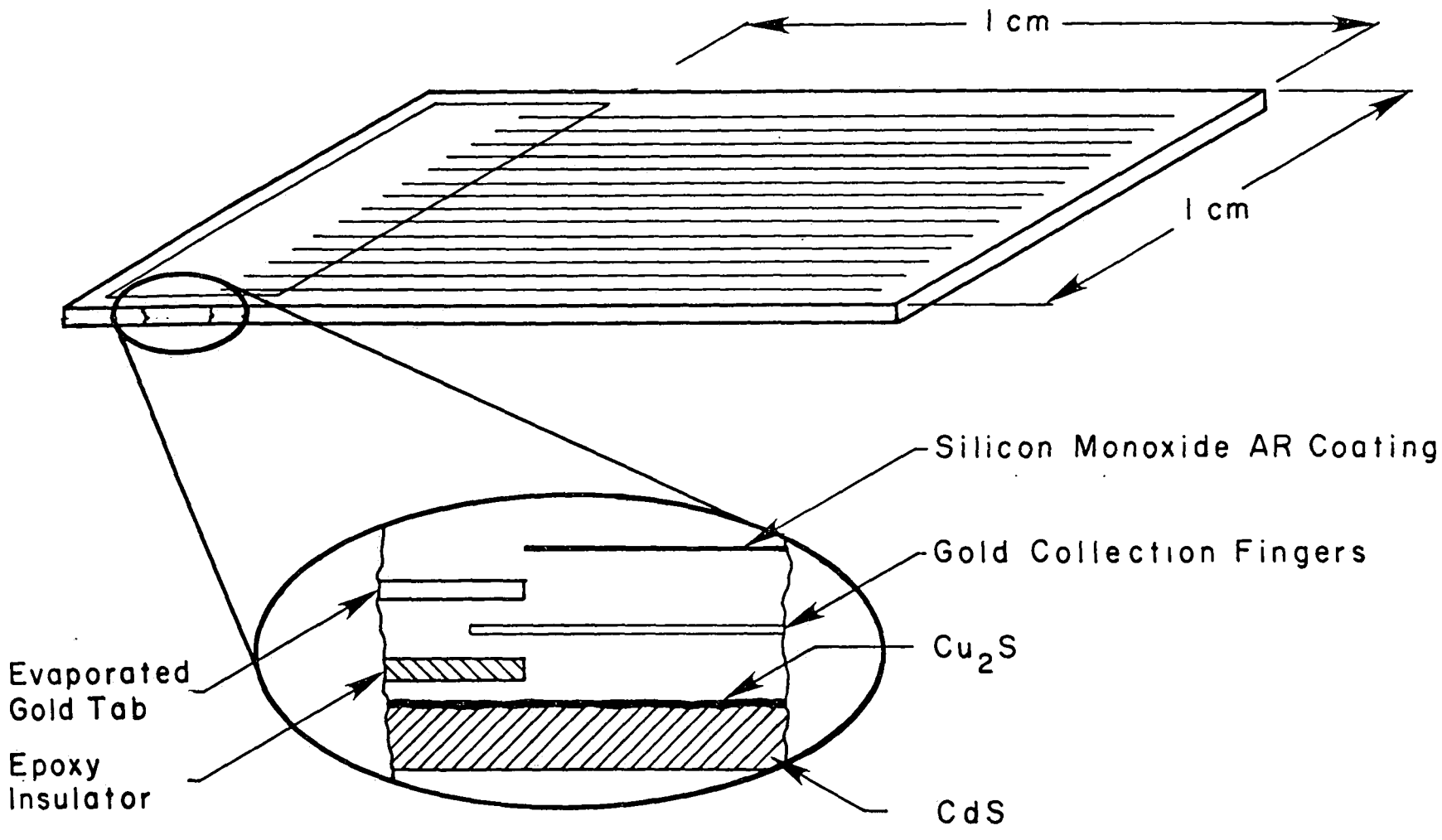

Figure 1. Design of an all-evaporated grid cell.

collection tab insulated with SiO. The data clearly shows the decrease in fill factor with increasing current typical for the 40 ℓpi grid.

Table 1

Simulated and Sunlight Tests for Cell #312-4A.
40 ℓpi Grid and SiO A-R Coating

Test	V_{oc} (V)	J_{sc} (mA/cm^2)	FF (%)	Eff (%)
W-I AM1 equiv.	0.48	20.7	62.0	6.20
Global Sunlight (82.3 mW/cm^2)	0.48	21.9*	65.9	6.90
Collimated Sunlight (69.8 mW/cm^2)	0.48	21.6*	67.1	6.90

*Adjusted to 100 mW/cm^2

As changes in gridding and A-R coatings are made, a quality control check on the basic cell production parameters (CdS deposition, Cu_2S formation, etc.) is maintained by simultaneously producing monitor cells. These are 2 x 2 cm cells with a conventional laminated 10 x 60 ℓpi grid. (All else being equal, a W-I simulator efficiency for these cells of 6.0% corresponds to a sunlight test efficiency with our best gridding and A-R of ∿ 8.2%.) Using the monitor cells a deliterious effect of aging of the HCl bath has been detected as is evident from examination of Table 2. Standard operating procedures have now been amended to include renewal of the 55% HCl bath after each 15 substrates (900 cm^2 CdS).

Table 2

The Influence of Etching on Cell Performance, Each Data Point is the Average for Three Cells

Process	V_{oc} (V)	J_{sc} (mA/cm^2)	FF (%)	Eff (%)
No etch	0.50	13.8	70.3	4.85
Aged HCl	0.51	15.4	64.7	5.45
Fresh HCl	0.51	16.1	70.9	5.82

Since September 1976, bulk resistivity has been measured on each substrate in order to monitor the CdS during ongoing experiments. During the October-December period, 25 CdS substrates were measured, with the distribution of resistivities shown in Figure 2. The distribution is fairly narrow, with only three of the 25 resistivities lying substantially outside the main distribution.

The bulk resistivity variation on a given substrate was also measured, and is shown in Figure 3. The distribution is symmetrical, with a slight increase toward the outer edges. (The true outer values are slightly higher than indicated since the film is thinner in those regions. A uniform thickness was assumed for the calculations.) Even so, the resistivity spread on a given substrate is considerably less than that seen between the substrates. Results to the present have shown no correlation between current density (or other cell parameters) and CdS resistivity. This indicates that at the present level of cell development the resistivity has, at most, a second order effect on cell response, at least for resistivities in the 0.5-5.0 Ω cm range.

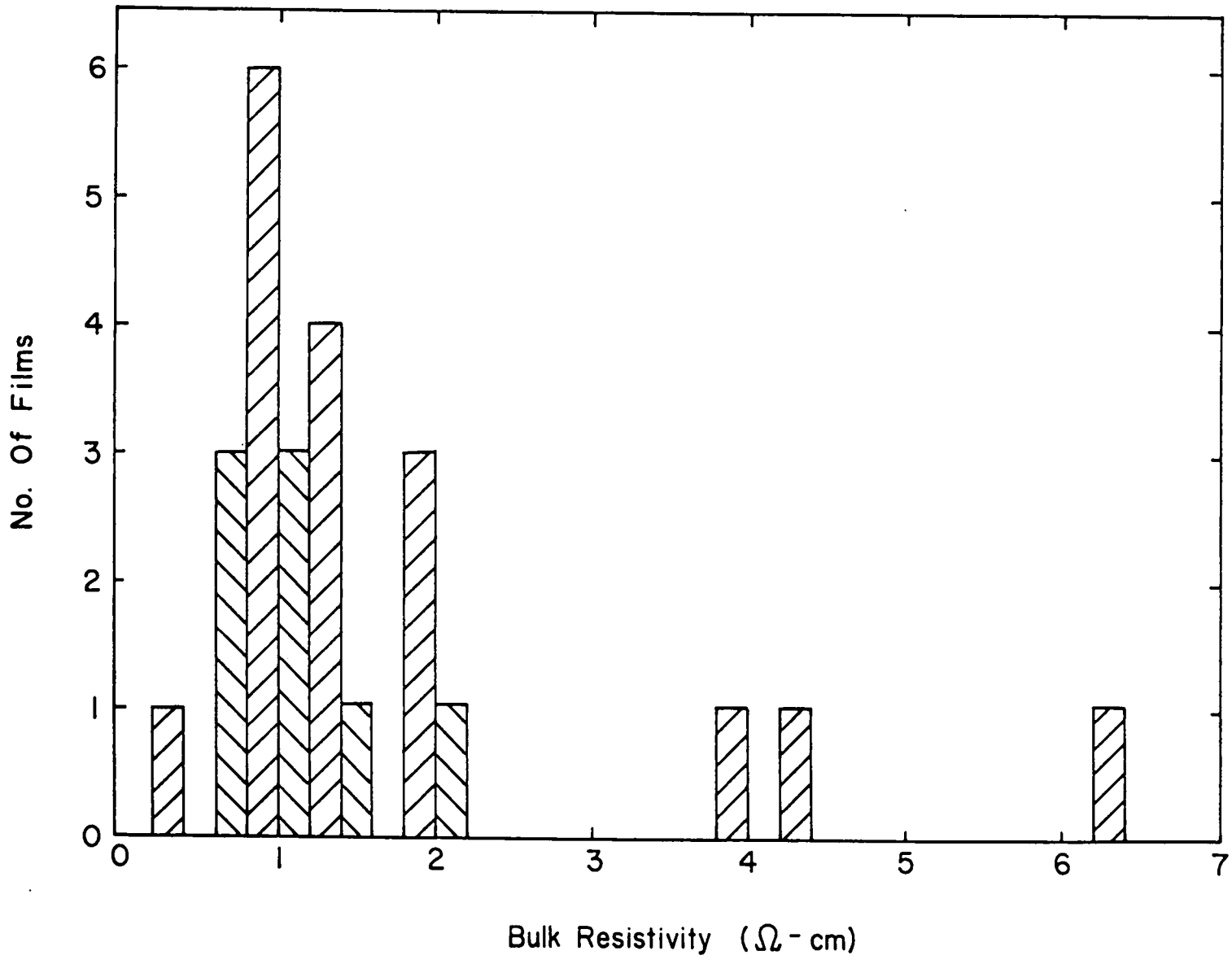

Figure 2. Distribution of CdS substrate resistivities for 25 substrates.

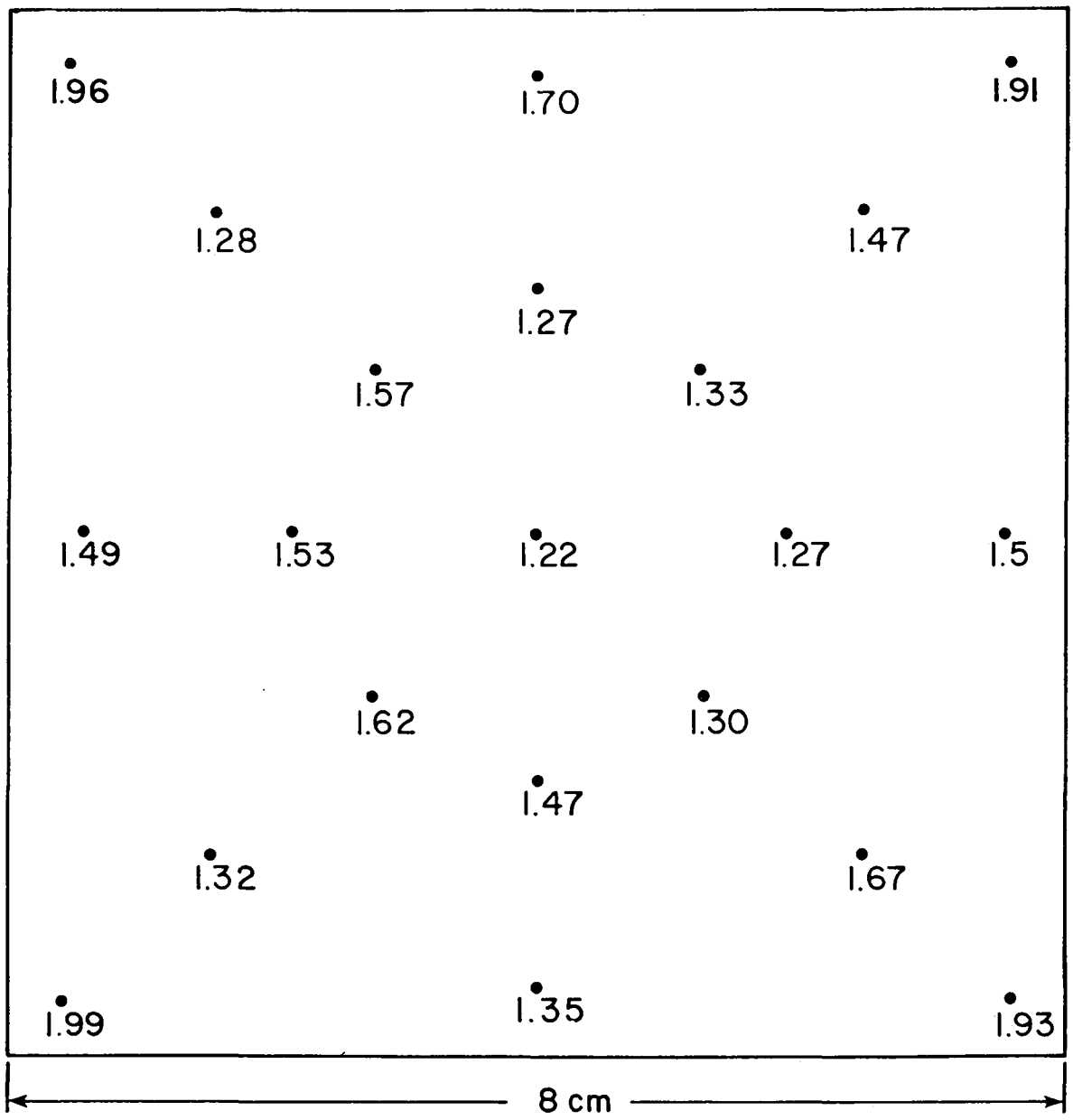

Figure 3. Variation in resistivity (Ω cm) across a CdS substrate.

An indication of the cell distribution to be expected from a single substrate can be seen in Table 3, where 24 cells (1.5 cm^2 area) were processed from the same substrate.

Table 3

Variation in Monitor Cell Parameters from Substrate #361. Total Number of 1.5 cm^2 Cells is 24; W-I Simulation Testing.

Parameter	Range	Average	Std. Dev.
V_{oc} (V)	.490-.505	.501	.005
J_{sc} (mA/cm)	14.16-16.99	15.75	.75
FF (%)	65.9-71.4	69.8	1.2
Efficiency (%)	4.67-6.10	5.52	.33

The production of Cu_2S by solid state reaction with vapor deposited CuCl (dry process) was selected for the (CdZn)S program. This was principally to ensure a uniform thickness of Cu_2S on substrates with a lateral gradient in zinc concentration. During this quarter a number of experiments have been conducted to generate comparative data between "wet" and "dry" CdS/Cu_2S cells. The study is not yet complete but some definite trends have been established. On unetched CdS the dry process gives a significantly enhanced V_{oc} with a maximum value of 0.54 V. Short circuit currents are lower for all unetched CdS because of the increased reflection losses. Results for etched and unetched CdS are given in Tables 4 and 5 respectively. If the Cu_2S is formed using the conventional solution reaction the currents are generally higher than for the solid state reaction. Comparative results are given in Table 6. It is not possible to draw firm conclusions about the ultimate achievable currents with the dry process as extensive current optimization has not yet been conducted on the dry process cells.

Table 4

Cell Parameters for CdS/Cu_2S Cells Made by Solid State Reaction on Un-etched CdS. W-I Simulation.

Cell #	Cu_2S Thickness (Å)	V_{oc} (V)	J_{sc} (mA/cm^2)	FF (%)	EFF (%)	Condition
358C1	1900	0.51	12.2	64.1	3.95	As gridded
			J_L = 14.5*			H_2/Ar H.T.
358C2	1900	0.51	11.7	65.9	3.91	As gridded
360B1	2900	0.52	11.7	70.7	4.24	As gridded
360B2	2400	0.52	11.5	71.6	4.23	As gridded
			J_L = 13.0			H_2/Ar H.T.
366B1	1400	0.52	12.8	70.2	4.69	As gridded
			J_L = 14.7			Vacuum H.T.
366B2	1400	0.52	12.2	70.6	4.48	As gridded
			J_L = 13.8			H_2/Ar H.T.
375C1	928	0.54	13.0	72.2	5.02	As gridded
		0.54	12.7	67.0	4.00	Vacuum H.T.
375C2	928	0.54	13.1	68.6	4.83	As gridded
		0.54	12.6	63.1	4.28	Vacuum H.T.

H_2/Ar heat treatment - 17 hours at 150°C

Vacuum heat treatment - 17 hours at 170°C

*J_L, light generated current is given when I-V shows hysteresis

Table 5

Cell Parameters for CdS/Cu_2S Cells Made by Solid State Reaction on CdS Etched in 55% HCl at 60° for 4 Seconds. W-I Simulation.

Cell #	Cu_2S Thickness (Å)	V_{oc} (V)	J_{sc} (ma/cm^2)	FF (%)	EFF (%)	Condition
360A1	2600	0.50	13.3	67.3	4.44	As gridded
			J_L = 15.23			Vacuum H.T.
360A2	2600	0.51	14.71	68.7	5.10	As gridded
			J_L = 16.3			H_2/Ar H.T.
366A1	1452	0.50	15.1	64.2	5.23	As gridded
			J_L = 16.8			Vacuum H.T.
366A2	1452	0.50	15.1	69.6	5.24	As gridded
			J_L = 10.5			H_2/Ar H.T.

H_2/Ar heat treatment - 17 hours at 150°C

Vacuum heat treatment - 17 hours at 170°C

J_L, light generated current is given when I-V shows hysteresis

Table 6

Comparison between CdS/Cu_2S Cells Produced by Solution and Solid State Reaction

	Solution		Solid State		
Cell #	J_{sc} (mA/cm^2)	V_{oc} (V)	J_{sc} (mA/cm^2)	V_{oc} (V)	Condition
		Unetched CdS			
327	13.8	0.50	12.5	0.53	As gridded
	15.4		14.9	-	Heat treated
358			12.2	0.51	As gridded
			14.2	-	Heat treated
360			11.6	0.52	As gridded
366			12.8	0.52	As gridded
375			13.0	0.54	As gridded
		Etched CdS			
358	15.2	0.50			As gridded
	18.2	-			Heat treated
300	15.5	0.49	14.7	0.51	As gridded
			16.3	-	Heat treated
366	15.1	0.51	15.1	0.50	As gridded
375	16.0	0.50			As gridded

The significantly enhanced V_{oc} justified further development of the solid state process with the addition of A-R techniques to reduce the reflection losses from the unstructured Cu_2S surface. There is no significant difference in voltage between the two Cu_2S formation processes on etched CdS. Optical microscopy reveals no detectable grain boundary invasion of Cu_2S for the solid state reaction and it is concluded that the significantly more planar junction resulting from the no etch-solid state reaction is responsible for the higher V_{oc}.

5.2 Development of (CdZn)S/Cu_2S Cells

Several (CdZn)S substrates were processed using both the solution and solid state techniques.[3] Cell results are summarized in Figures 4 and 5 where current density and open circuit voltage are plotted as functions of zinc composition. (None of the (CdZn)S layers represented in these figures were etched.)

For dry processed cells, V_{oc} is usually in the .67-.68 volt range for zinc content above the 10%. The wet processed cells do not exhibit V_{oc} this large until about 40% zinc. As seen in the figures, the higher V_{oc} values for both wet and dry processed cells are accompanied by a decrease in current density. The majority of cells show some time dependent current-voltage characteristics which are strongly dependent on fabrication history. Heat treatments have a particularly marked effect on the stability of the I-V.

The magnitudes of J_{sc} should be compared to 12-13 mA/cm^2 for CdS cells with the same gridding and surface treatments (see Table 4). There

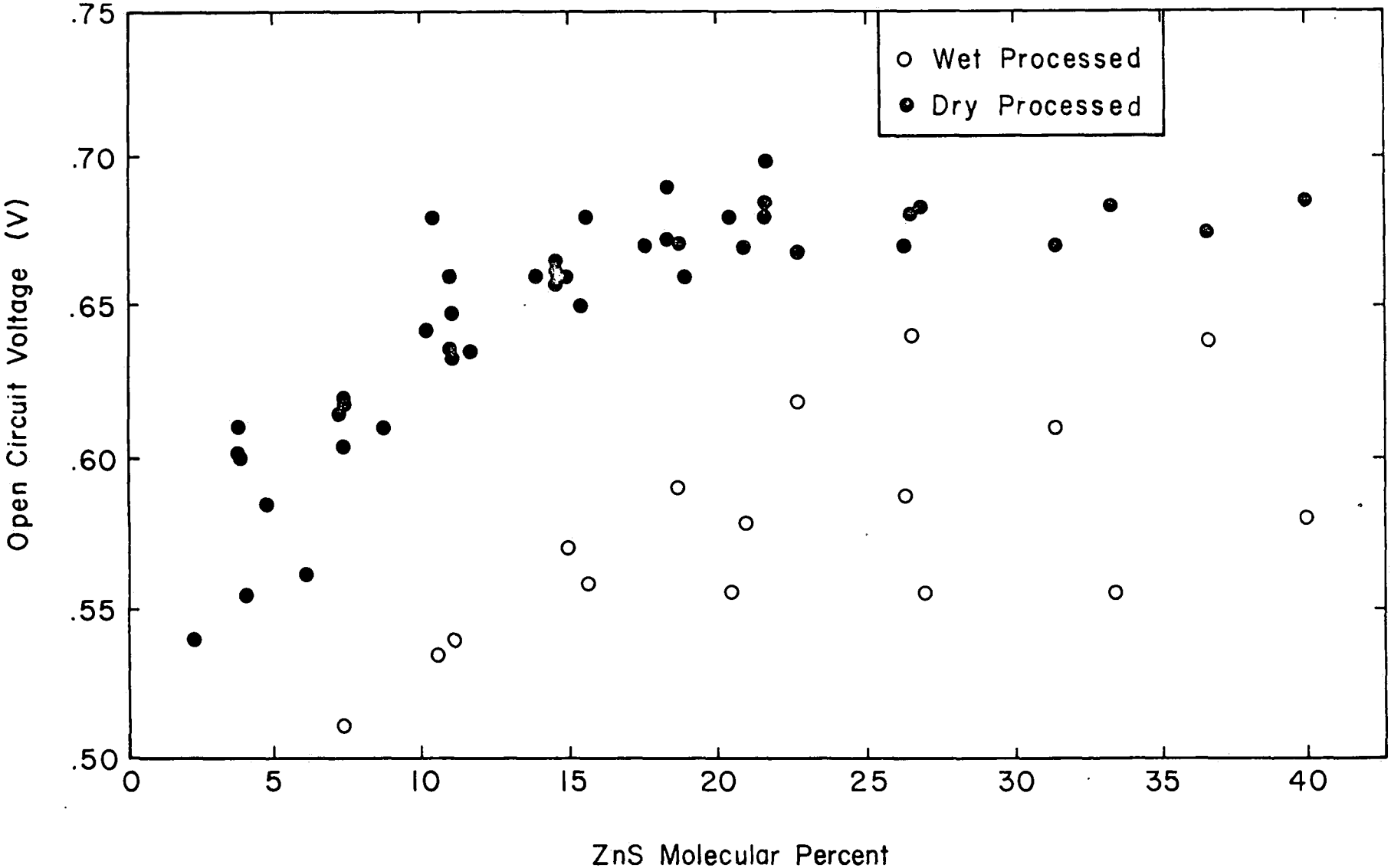

Figure 4. Open circuit voltage as a function of zinc content for (CdZn)S/Cu_2S cells given no post gridding heat treatment.

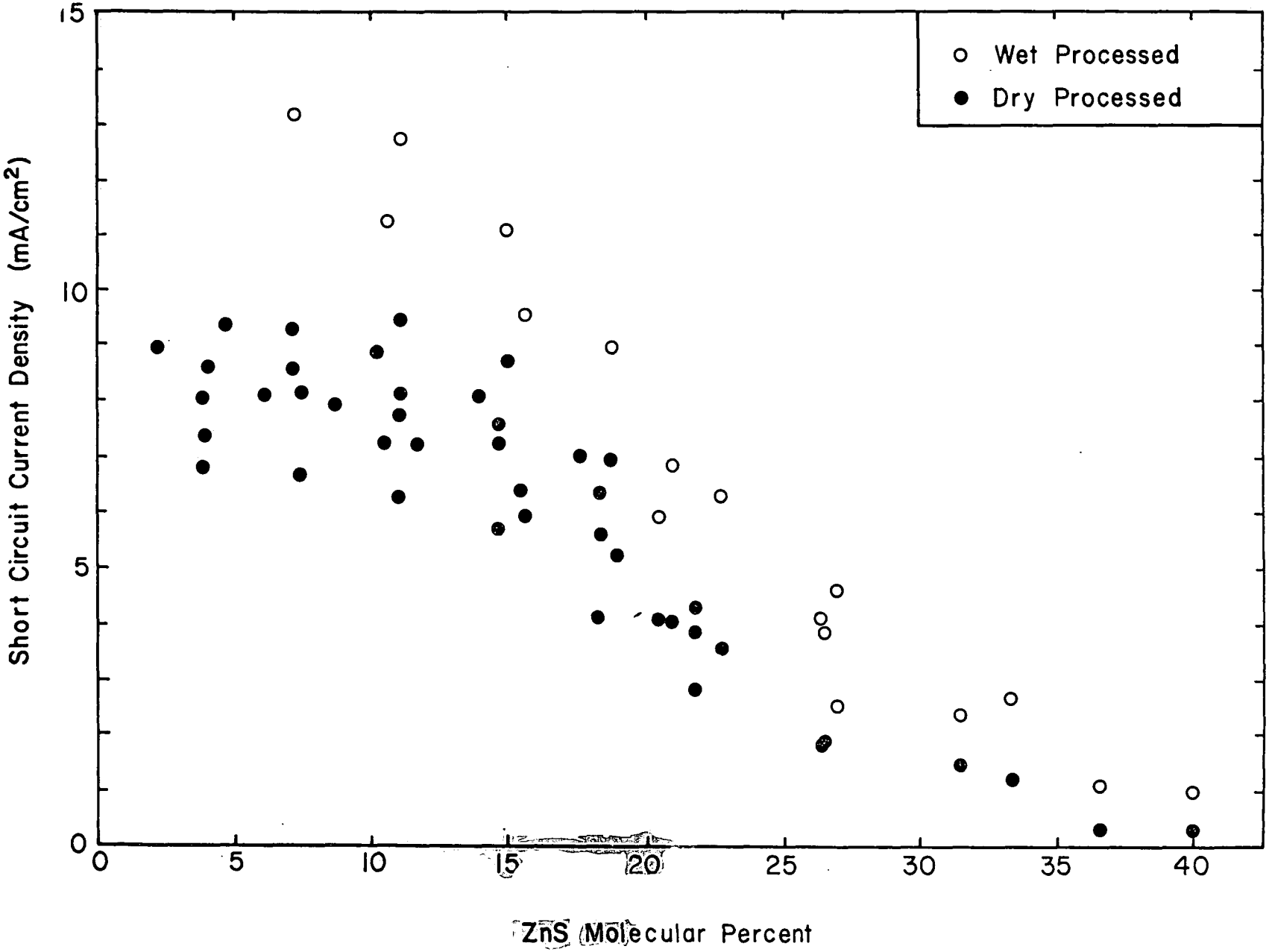

Figure 5. Short circuit current as a function of zinc content for (CdZn)S/Cu_2S cells given no post gridding heat treatment.

are several possible mechanisms that can account for the decrease in J_{sc} as zinc content is increased and these are discussed in Section 5.4.

In general, the mixed sulfide films have higher resistivities than the CdS. This could reduce the current collection efficiency at the junction by directly influencing the electric field strengths. The bulk resistivity of the mixed sulfide films (for $\lesssim$ 10% zinc) has been reduced to less than 20 Ω cm by increasing the film deposition rate to over 4 microns/minute. Etched CdS layers in this resistivity range have yielded current densities over 16 mA/cm^2 (W-I simulation), and it is concluded that this parameter is not solely responsible for the present current levels. The combination of an appropriate etch to reduce reflection, and an optimum heat treatment, should result in current densities of over 15 mA/cm^2 for the testing and gridding procedures presently being used on these early (CdZn)S/Cu_2S cells, i.e., 80% grids and W-I simulation.

Initial heat treatments of 16 hours at a pressure of 350 μm and temperature of 170°C have been performed on several dry process mixed sulfide cells. The highest current densities for unetched mixed sulfide cells with 10 x 60 80% transparent grids were obtained using this technique. Open circuit voltage and short circuit current density before the heat treatment (open circles) and after (closed circles) are plotted in Figure 6. These currents should be compared to those seen in Table 4 for unetched CdS cells that have been dry processed. The current densities for some of the better mixed sulfide cells are in the same range as for CdS made under similar conditions. It is anticipated that a textured (etched) mixed sulfide surface will result in current density increases

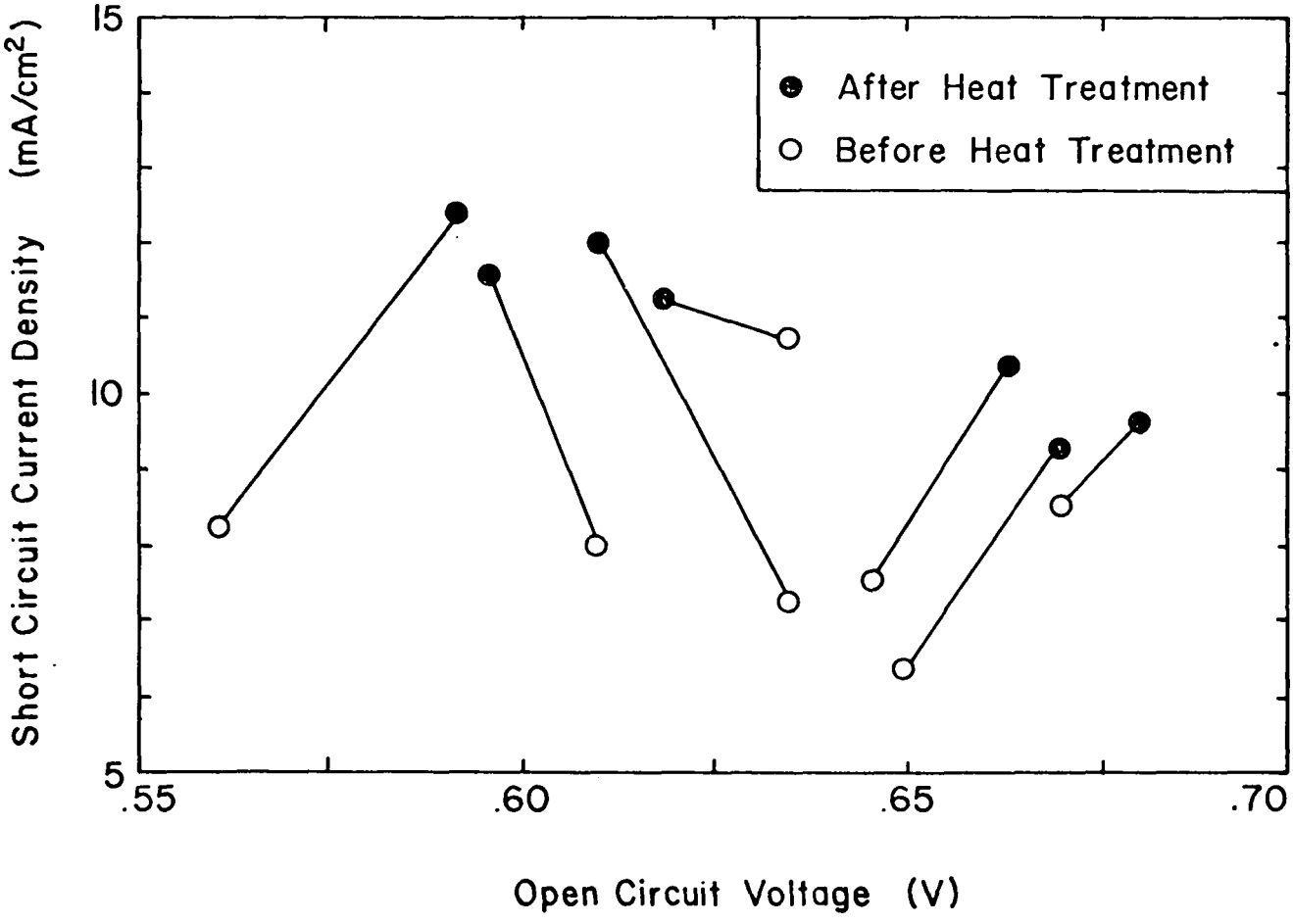

Figure 6. The relation between short circuit current and open circuit voltage for (CdZn)S/Cu_2S cells of various compositions.

of ∿ 20%, as was the case for dry processed CdS (Table 4). Heat treatment and etch tests are currently in progress.

Cells Measured at NASA-Lewis

In December 1976, cells were processed from five substrates using the solid state technique (unetched). Five cells were sent to NASA-Lewis to be measured. The cell parameters for these five cells are given in Table 7. The Delaware (IEC) measurements were made under W-I illumination callibrated with NASA-Lewis CdS cell C-9. The NASA-Lewis measurements were made under Xenon simulation calibrated to AM1 equivalent using CdS reference cell Z-67.

Table 7

Comparison of Mixed Sulfide Cell Parameters Measured at IEC and at NASA-Lewis on 12/17/76. First Values are IEC - Second, NASA-Lewis.

Cell #	V_{oc} (V)	J_{sc} (mA/cm^2)	FF (%)	EFF (%)	Grid
377S2	.58	12.0	63.5	4.44	Hybrid (evaporated & laminated)
	.57	12.2	61.0	4.29	
376A4	.66	10.2	61.8	4.16	10 x 60
	.65	10.7	60.7	4.23	
385A3	.62	11.2	53.8	3.80	10 x 60
	.57	11.0	Unstable		
386B5	.62	12.2	61.0	4.60	10 x 60
	.60	12.0	57.8	4.20	
377S1	.56	13.0	63.5	4.64	Hybrid
	.57	13.5	60.6	4.70	

These measurements verify that J_{sc} values over 12 mA/cm^2 with a V_{oc} over 0.6 V can be obtained.

5.3 Cu_2S Films

A project has been initiated with the short term goal of studying the electronic and optical behavior of Cu_2S films that are not part of a CdS/Cu_2S heterojunction. The first efforts were to produce Cu_2S films by electrochemical treatment of copper. Cu_2S films were formed by anodizing electropolished copper foil ($\sim$ 1.5 mils thick) in an aqueous sulfide media; the resulting film thicknesses were 0.1-0.5 microns. The films were then annealed in a hydrogen-argon atmosphere at $\sim$ 150°C. From the Cu-S phase diagram, copper sulfide equilibrated with metallic copper should be stoichiometric and should have the highest intrinsic resistivity (lowest carrier concentration). Metal contacts (Al, Au, Sn, Zn), typically .001 cm^2 in area, were thermally evaporated onto the copper sulfide at a pressure $\leq 5 \times 10^{-7}$ torr. These contacts invariably showed ohmic behavior. *In situ* heat treatments immediately following metallization (30-60 minutes at 150°C) failed to have any effect. Examination of the Cu_2S films by scanning electron microscopy revealed discontinuities in the Cu_2S films that were at least one micron in lateral extent. The copper foil substrate was visible through these defects. Thicker Cu_2S layers appeared to have fewer defects. Nevertheless, evaporated Al contacts on 5 micron thick anodically formed Cu_2S exhibited the same ohmic behavior as on the thinner films.

Experiments planned for the third quarter will focus on alternate film formation procedures to produce continuous, defect free Cu_2S layers.

5.4 Electro-Optical Analysis

Sheet Resistance of Cu_2S by van der Pauw Technique

One of the most important parameters of Cu_2S based cells is the resistivity ρ (usually measured as sheet resistance ρ/d) of the Cu_2S layer. The sheet resistance enters into cell operation directly through the series resistance of the cell. There is also a known correlation between high values of ρ/d and high values of short circuit current in the cell. High ρ/d values have also been shown to be correlated with higher optical absorption in the Cu_2S layer.

In the past the sheet resistance of the Cu_2S layer was measured using a four point probe on bare Cu_2S on CdS. This gave the value of ρ/d at that stage of the processing of the cell but did not give the value of ρ/d appropriate to the Cu_2S in the cell after lamination and subsequent heat treatments. In order to follow easily the changes in sheet resistance which occur during the lamination and heat treatment of cells, van der Pauw samples were prepared as indicated in Fig. 7. In Fig. 7a, four gold plated Cu tabs were laminated to the Cu_2S in the same way that the grid contact is formed in laminated cells. A portion of the surface was left bare so that four point probe values could be obtained from this region.

To obtain ρ/d from the van der Pauw samples current is passed through contacts A and B (current I_{AB}), and the voltage drop measured between contacts D and C (V_{DC}), then current is passed through contacts A and D (I_{AD}) and the voltage measured between B and C (V_{BC}). The expression for ρ/d is

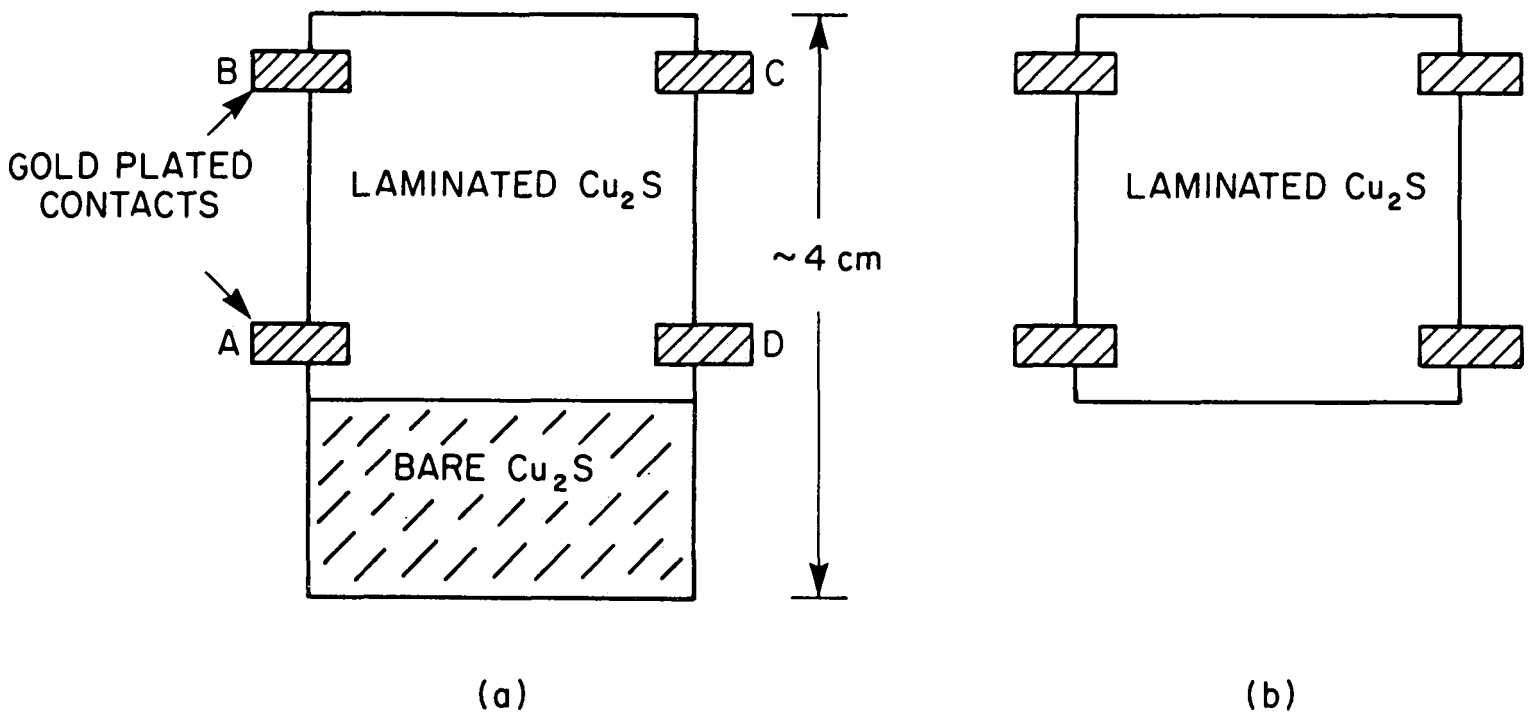

Figure 7. Contact configuration for van der Pauw sheet resistance technique.

$$\frac{\rho}{d} = \frac{\pi}{2\ell n2} \left(\frac{V_{DC}}{I_{AB}} + \frac{V_{BC}}{I_{AD}}\right) f$$

where f is a correction factor which takes into account the non-symmetric placement of the contacts. For our sample, $f \simeq 1$, and the ratios V_{DC}/I_{AB} and V_{BC}/I_{AC} should be approximately equal to one another if ρ/d is uniform. Measurements must be taken in the absence of light to prevent errors due to the light generated currents.

In practice I_{AB} and I_{AD} were equal, usually 10 μa and the ratio V_{DC}/V_{BC} gives an indication of the non-uniformity of ρ/d. In Table 8, the evolution of the ρ/d values for a sample of Fig. 7a design is given. The bare region values of ρ/d decay more rapidly than laminated regions. The inhomogeneity in laminated region ρ/d become severe particularly after heating in air. The ρ/d value was obtained as a function of temperature for this sample to see whether the crystallographic change in chalcocite could be seen. Due to the bare region and the inhomogeneity of the sample no transition was seen in this sample. Four samples for resistivity studies were prepared from substrate 378 which is dry dip Cu_2S on $Cd_{1-x}Zn_xS$, with x ranging from .05 to .18 as one goes from sample 378-1 to 378-4. Table 9 gives a summary of the results for these samples. Fig. 8a shows ρ/d a function of temperature for sample 378-1 on 11/12/76, and Fig. 8b shows 378-1 on 11/24/76. A discontinuity marks the phase change. Considerable hysteresis between the heating and cooling curves are observed. Part of this is due to the supercooling of the phase transition; the lower values of ρ/d after heating is due to an actual change in stoichiometry of Cu_2S due to oxidation of the Cu_2S layer to form a Cu_2O layer on the surface. The H_2-Ar heat treatment reduces the Cu_2O to free Cu which diffuses into

Table 8

Development of Cu_2S Sheet Resistance with Storage and Heat Treatment. The van der Pauw Measurement is for a Cu_2S under an Epoxy-aclar Lamination. The Four Point Probe Measurement is on Cu_2S Exposed to the Atmosphere.

Date	V_{DC}/V_{BC}	ρ/d (van der Pauw)	ρ/d Four Point Probe
9/23/76	2.1	5.7×10^3 ohms	6.9×10^3 ohms
9/24/76			4.8×10^3 ohms
9/27/76	2.6	5.5×10^3 ohms	3.2×10^3 ohms
9/30/76	2.1	5.1×10^3 ohms	
	Heated to 100°C in air		
10/6/76	3.7	4.15×10^3 ohms	
	Two regions separated		
10/7/76	23.1	3.6×10^3 ohms	$\sim 0.8 \times 10^3$ ohms

Table 9

Influence of Air Storage and Heat Treatments on the Sheet Resistance of the Cu_2S Layer on Series 378 Cells

Sample	Date	T(°C)	(10^3 ohm) ρ/d	$\frac{V_{DC}}{V_{BC}}$	Heating T_T (°C)	Cooling T_T (°C)	at 30°C 10^3 ohm ρ/d	$\frac{V_{DC}}{V_{BC}}$
378-1	11/11/76	26.7	5.79	1.1				
378-2	11/11/76	26.7	6.58	1.2				
378-3	11/11/76	26.7	6.85	1.7				
378-4	11/11/76	26.7	9.74	1.5				
378-1	11/12/76	26.7	5.63	1.1	102	70	2.19	1.25
378-2	11/15/76	25.0	6.23	1.1	102	70	3.94	1.24
378-3	11/16/76	30.0	6.09	1.8	102	70	4.16	1.72
378-4	11/17/76	25.0	7.29	1.3	103	70	4.49	1.52
378-1	11/22/76	21.5	2.47	1.3				
378-2	11/22/76	21.9	4.29	1.1				
378-3	11/22/76	22.0	4.54	1.6				
378-4	11/22/76		OPEN					
			AFTER 15 HR. H_2-Ar AT 150°C					
378-1	11/23/76	19.1	48.4	.96				
378-2	11/23/76	19.3	47.9	1.1				
378-3	11/23/76	19.5	33.0	2.5				
			4 HRS. IN DESSICATOR AND 14 HR. IN H_2-Ar AT ROOM TEMP.					
378-1	11/24/76	20	11.2	1.0	103	70	3.47	1.37

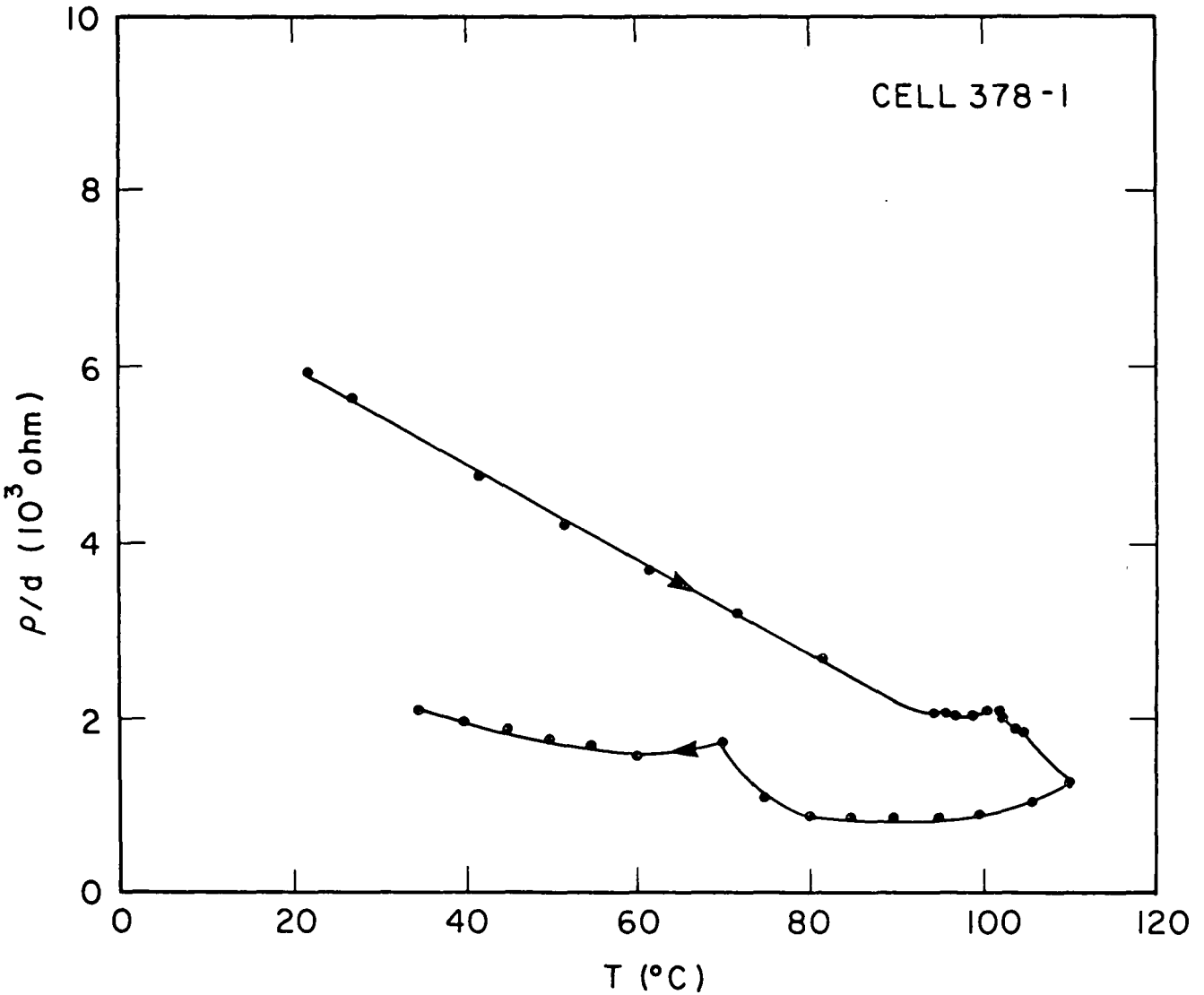

Figure 8a. Influence of a temperature excursion on Cu_2S sheet resistance. Test performed 11/12/76, see Table 9.

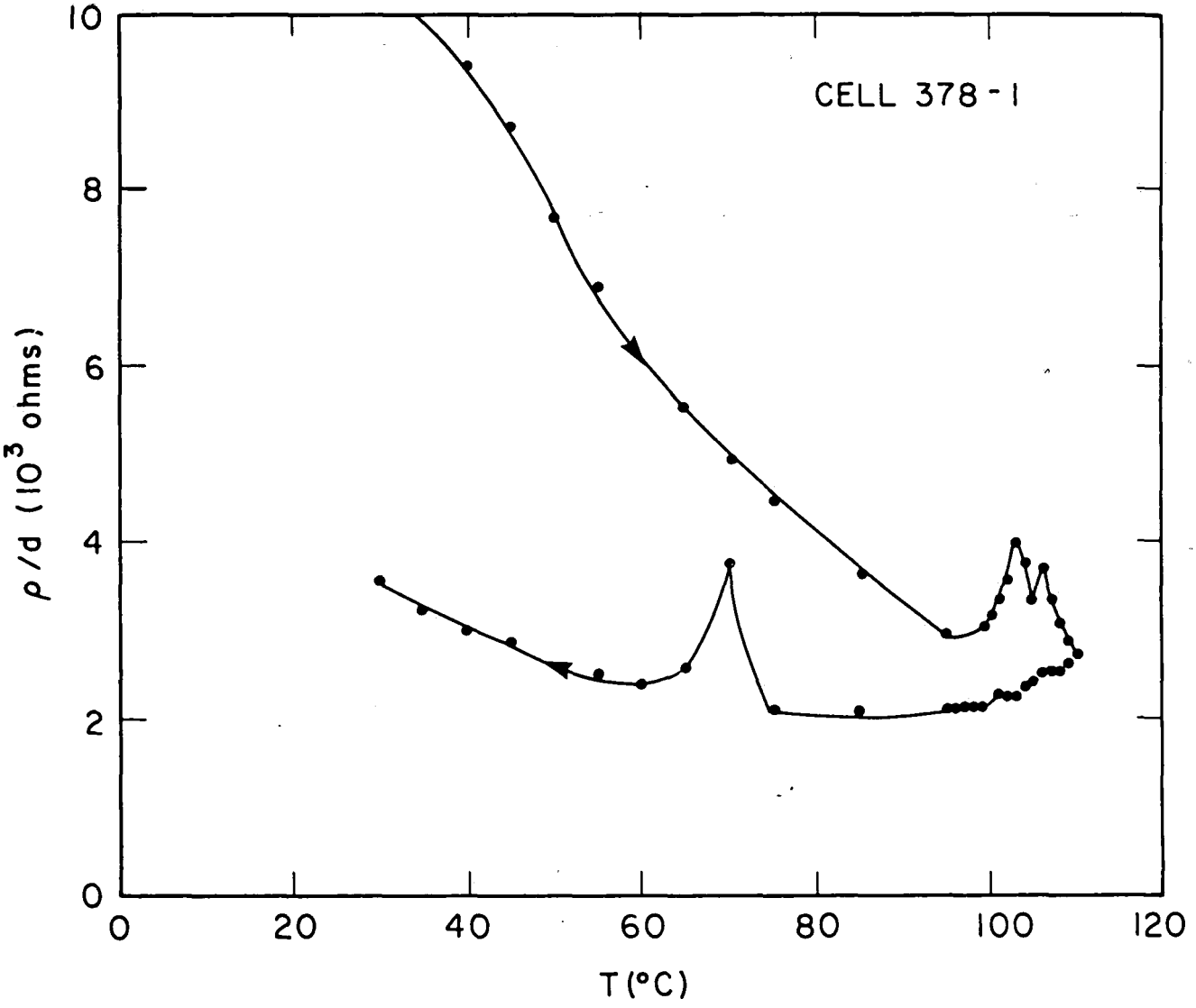

Figure 8b. Influence of a temperature excursion on Cu_2S sheet resistance. Test performed 11/24/76, see Table 9.

the Cu_2S to increase the stoichiometry and give dramatic increases in ρ/d by factors of 10 or more. Exposure to air again decreases ρ/d and heating in air decreases ρ/d at a faster rate.

The structures in ρ/d seen in Figure 8 are characteristic of all the samples. The higher the initial value of ρ/d the more pronounced is the peaks at 102°C on heating and at 70°C on cooling.

These studies are directly related to the properties of laminated cells since the van der Pauw samples are processed in the same way as the cells. The series resistance of the cell is related to ρ/d by the relation

$$R_s A = \frac{\rho}{12d} S^2$$

where A is the area of the cell and S the spacing between grid lines assuming a parallel line grid. The value of $R_s A$ found in good cells is in the range of 1 ohm-cm in cells with grid contacts 10 x 60 lines per inch. Such a range is consistent with R_s being wholly due to the sheet resistance of Cu_2S with $\rho/d \simeq 6.7 \times 10^3$ ohm, which is within the range of values seen in Tables 8 and 9.

Fill Factor for Parallel Line and Square Grids

In a previous progress report[1] we reported the result that the loss in fill factor due to series resistance was given by the relation

$$(\Delta FF)_{R_s} = \frac{-j_{sc} R_s AC}{V_{oc}}$$

where j_{sc} is the short circuit current density, R_s the series resistance, A the area of the cell and C a factor which depends on V_{oc}/kT; for T = 300°K, and, V_{oc} = 0.5, C ≃ 0.9. The expressions for R_sA for parallel line grids and square grids due to sheet resistance are

$$(R_sA)_{par} = \frac{\rho}{d} \frac{S^2}{12}$$

and

$$(R_sA)_{sq} = \frac{\rho}{d} \frac{S^2}{32}$$

where S is the spacing between grid lines.

Using typical values V_{oc} = 0.5V, j_{sc} = 0.02 A/cm^2 and $\rho/d = 10^4$ ohm, we have

$$(\Delta FF)_{R_s} \text{ par} = 30\ S^2$$

$$(\Delta FF)_{R_s} \text{ sq} = 11.25\ S^2$$

with S in cm. Cells also have a loss in fill factor due to the variation in j_L with voltage. For typical cells this value is on the order of ∿ 0.05. Three types of grids have been studied recently. These are laminated grids with 60 lines/inch x 10 lines/inch, evaporated grids with 40 lines/inch, and cross gridded cells with evaporated grids 40 lines/inch, with a laminated grid at right angles to the evaporated one of 40 lines/inch. The 60 ℓpi x 10 ℓpi can be considered to be a parallel line grid of 60 ℓpi for calculation purposes, since the 10 ℓpi grid makes only a small change in R_s. In Table 10 we list the three types of grids and the expected fill factors. For a cell with open circuit voltage of 0.5 V at

Table 10

Fill Factor for Various Grids with $(\Delta FF)j_L = -.05$, $j_{sc} = 0.02$ A/cm^2, $V_{oc} = 0.5$ V

Grid	$(\Delta FF)_{R_s}$ $\rho/d = 10^4$ ohm	FF	$(\Delta FF)_{R_s}$; $\rho/d = 5 \times 10^3$ ohm	FF	FF_{expt}
60 x 10 (S = .042 cm)	.053	.70	.027	.73	.689
40 (S = .0635 cm)	.123	.63	.062	.69	.720
40 x 40 (S = .0635 cm)	.045	.70	.023	.72	.727

300°K, the ideal fill factor is 0.80. The last column in Table 10 is the experimental FF for the highest efficiency cell of each type.

Factors which can raise the observed fill factor are lower ρ/d and lower j_{sc}; the fill factor will be lowered by low shunt resistances and increases in the bias sensitivity of j_L. Since lower ρ/d also reduces j_{sc} substantially and $(\Delta FF)_{R_s}$ the observed FF can approach 0.75 in a cell of poor overall efficiency.

Short Circuit Current and Spectral Response of (CdZn)S/Cu_2S Cells

At present the (CdZn)S/Cu_2S cells show the higher open circuit voltages predicted by the theory of the cell, but the short circuit current still remains lower than expected. Investigations of mixed sulfide cells were undertaken in order to determine the cause of the decrease in short circuit current density with an increase in zinc content. A number of cells were made with Zn content spanning the range from 2% to 36.7% as determined from x-ray measurements. (These results are presented in Section 5.2.) It was found that the current density noticeably started to decrease for a zinc content greater than 10-12%. Measurements of the optical density as a function of wavelength gave an energy gap of approximately 2.49 eV[3] for this composition. With the assumption that only the energetic position of the conduction band changes with the change in Zn content, it is not expected that a band spike would appear until a Zn content of at least 25% (for example, see ref. 4) - i.e. for an energy gap of the mixed sulfide being approximately 0.20 eV greater than that of CdS. Therefore on the basis of these experiments, it was expected that the current loss is due to other than the appearance of a band spike.

A number of possible causes for the lower j_L values have been considered. These include (1) lower diffusion lengths due to Zn remaining in the Cu_2S layer, (2) a conduction band spike at the $(CdZn)S/Cu_2S$ interface due to an excess in Zn near the interface, (3) low electric field at the interface due to low carrier concentration in the (CdZn)S layer or (4) due to the lack of the ionization of deep levels near the junction, and (5) an increased interface recombination velocity due to an increase in the energy range available for recombination. Mechanism (2) was suggested by spectral response measurements (I_{sc} and photocapacitance vs. λ) which give an indicated energy gap that is considerably greater than that obtained from measuring the optical density. In CdS/Cu_2S cells a peak in collection efficiency as a function of wavelength occurs at a photon energy close to the band gap energy of the CdS. A similar peak is seen in the photocapacitance of CdS/Cu_2S cells. In the $(CdZn)S/Cu_2S$ cells the peak in both the spectral response and photocapacitance shifts to shorter wavelengths with increasing Zn. However, the peak occurs at wavelengths shorter than that corresponding to the band gap of the material as determined optically, and from x-ray determination of the lattice constant. Table 11 shows the results for several cells. The reduced precision in the peak position at high Zn concentrations is due to the noisiness of the light source at short wavelengths.

The spectral response measurements indicate, therefore, that a conduction band spike is the most likely reason for the decrease in short-circuit current density with increasing Zn content, with a region of

Table 11

Peaks in Spectral Response of CdS;and (CdZn)S

Cell	Type	%Zn (x-ray optical)	E_{peak} (eV)	$(E_p - E_{g_{CdS}})$ (eV)	%Zn (E_{peak})
8-2	CdS	0	2.455 ± .02	0	0
370D1	(CdZn)S	10.6	2.64 ± .02	0.18 ± .03	25 ± 3
370D3	(CdZn)S	21.0	2.755 ± .03	0.30 ± .04	42 ± 5
370D5	(CdZn)S	31.5	∿2.95	∿.5	∿60

enhanced Zn content near the junction accounting for the difference in Zn content deduced from spectral response and that obtained from x-ray and optical measurements.

However, some caution must be used in associating the peaks observed with the energy gap. In the spectral response, part of the peak is due to the direct generation of current in the CdS and part due to the enhanced field at the junction due to hole trapping in CdS. The peak in photocapacitance is due to the generation and trapping of holes in CdS. The magnitude of the peaks depends upon the efficiency of the light reaching the CdS, in creating holes, the density of hole traps and the amount of light reaching the CdS (or (CdZn)S). The amount of light reaching the CdS depends upon the strength of the light source in the appropriate wavelength range, the absorption coefficient of the overlying Cu_2S layer and the thickness of this layer. The direct generation of current in CdS, and the most efficient generation of holes in CdS must occur for wavelengths less than that of the CdS band gap. At shorter wavelengths, however, the absorption coefficient of the Cu_2S rises, and the strength of the light source is decreasing. These latter factors tend to confine the peak to wavelengths close to that of the energy gap. This would tend to be more the case for thicker Cu_2S layers. If the Cu_2S became thick enough the peak might even shift to wavelengths longer than that of the band gap and simply be the peak in the product of the amount of light reaching the CdS and the efficiency of trapping holes.

The above discussion supports the contention that the peaks seen are close to the band gap of the CdS (or (CdZn)S). A possible situation

exists in which the peak could occur at considerably shorter wavelengths than the band gap. Although the onset for pair creation in CdS occurs at the band gap wavelength the pairs are created at some depth into the CdS, corresponding to the absorption coefficient variation with wavelength. For the direct current from CdS to be seen, the holes generated must reach the Cu_2S before recombining or being trapped. For the photocapacitance to be observed holes must be trapped in the space charge region near the junction. If the hole trap were located extremely close to the Cu_2S-CdS (or Cu_2S-(CdZn)S) interface and fast recombination occurred further into the CdS, then only highly absorbed light i.e. considerably shorter wavelength than the gap could contribute to trapping in these levels. The peak in both spectral response and photocapacitance would then occur at wavelengths shorter than the band gap wavelength.

In CdS/Cu_2S cells heat treatments lead to a progressively thicker compensated region near the junction. This region is believed to be due to the diffusion of Cu into the CdS. A decrease in capacitance and the increase in the cross over between light and dark curves both support this view. The hole traps are either at the Cu impurity site or associated with it. In (CdZn)S/Cu_2S cells capacitance and the cross over between dark and light I-V curves have not been studied in detail. However, it is known that in these cells the I-V curves do not respond to heat treatment in the same way that CdS cells do. Since the (CdZn)S has a smaller lattice constant than CdS, the diffusion coefficients determining the movement of Cu into the (CdZn)S layer might be much smaller than for CdS. Correspondingly longer heat treatments might then be necessary to

establish a compensated layer comparable to that which occurs in good CdS/Cu_2S cells. This situation would account for the peaks in spectral response and photocapacitance differing from the band gap deduced from lattice constant measurements. It would also account for the low j_L values through mechanism (4). Further studies will reveal which situation actually occurs.

Measurements of I_{sc} versus intensity showed a linear relationship for cell 370D1, with super linear behavior at higher Zn content.

Time Dependent Effects

Besson et. al.[5] have reported on the temporal instability of the open circuit voltage for CdS/Cu_2S cells that was solved by doping. CdS/Cu_2S cells produced at IEC have generally now shown this behavior. However, the temporal instability is present in mixed sulfide cells. Figure 9 shows an example of the decay for cell 376C-1. The decay appears to be associated with the effects of electron and hole trapping on the field at the interface, and, consequently, the interface recombination. Further experimental and theoretical studies are being made in order to determine more precisely the nature of the problem and to program solutions.

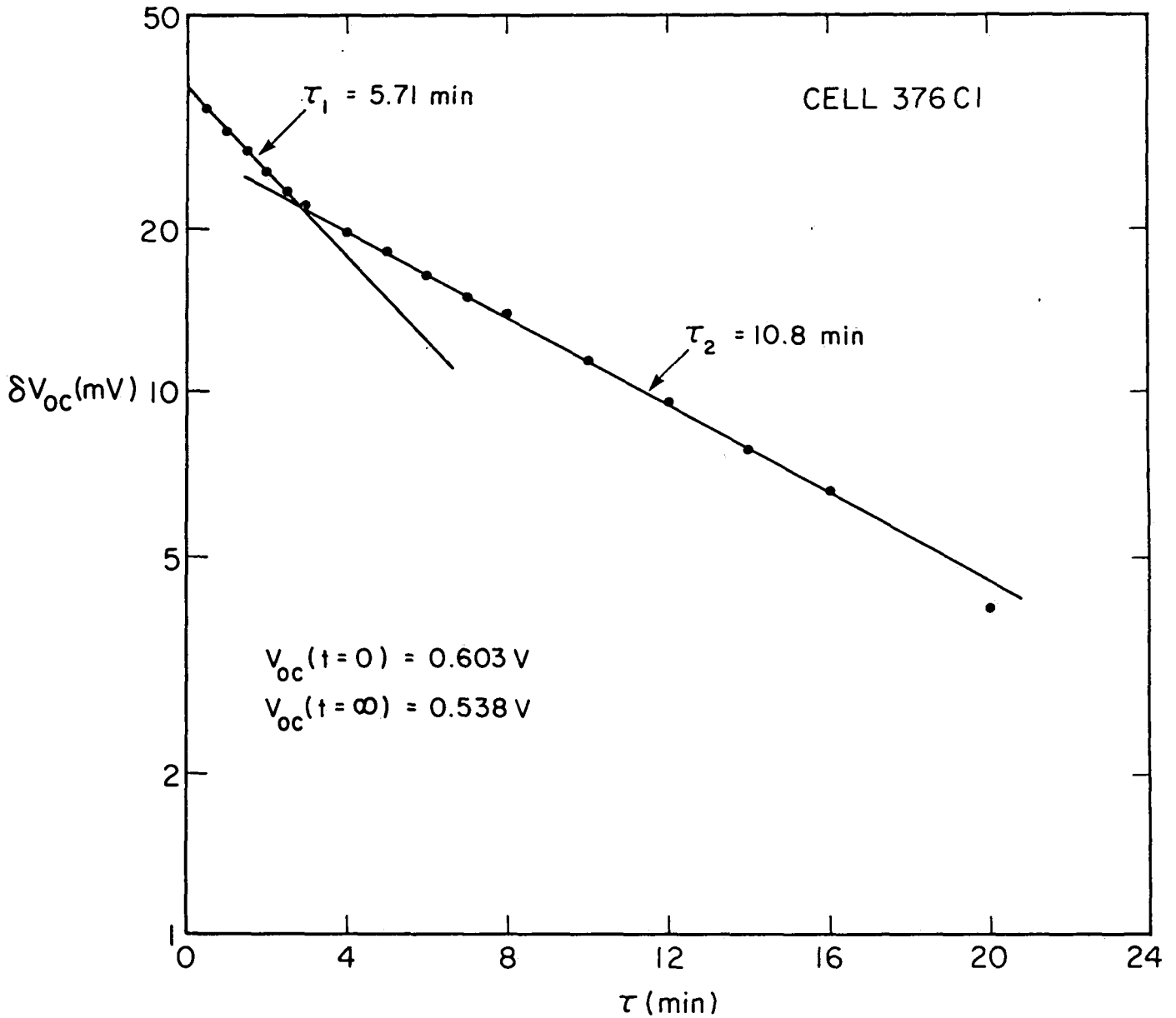

Figure 9. Open circuit voltage decay with time for (CdZn)S/Cu_2S cell #376C1.

5.5 Theoretical Analysis

Relation of Cu_2S Stoichiometry to CdS/Cu_2S Cell Properties

The stoichiometry of the Cu_2S layer is related to almost all aspects of the cell. A better understanding of these relationships and inter-relationships is essential to any optimization of cell design. In the absence of any other donor or acceptor levels, the Cu vacancy density determine the hole concentration through the relation p = [Cu] vac. If we write the stoichiometric relation $Cu_yS = Cu_{2-x}S$ we have

$$x = \frac{p}{2 \times 10^{22}}$$

The stoichiometry will thus control the resistivity of the Cu_2S layer through the relation

$$\rho = \frac{1}{q\mu_p p}$$

with μ_p the mobility of the holes. Since the Cu vacancies act as ionized scatterers, the mobility should also be a function of stoichiometry. Indeed both ρ and μ_p have been found to depend upon stoichiometry, quite strongly in some instances.[6] The short circuit current of the cells has also been found to vary strongly with the stoichiometry[7] of the Cu_yS. There are several possible causes for this. First the diffusion length of the generated electrons in Cu_yS should be affected. Since

$$L = (kT\ \mu_n\ \tau_n/q)^{\frac{1}{2}}$$

and both μ_n and τ_n can dependent upon $[Cu]_{vac}$ either directly or through the relation of $[Cu]_{vac}$ to p, j_L should vary with stoichiometry for this reason. A further possible variation in j_L arises due to the changes in

the absorption coefficient with stoichiometry.[8-9] Such changes are seen in the wavelength region in which the cell responds as well as in the infrared region, at wavelengths longer than the Cu_yS band gap.

There is also cathodoluminescence data on samples of Cu_yS[10] prepared in various ways which may also be interpreted by similar considerations.

We have also previously calculated[1] the expected variation in V_{oc} as a function of Cu_yS stoichiometry due to shifts in the Fermi level of the Cu_yS and band bending in the Cu_yS layer.

The changes in cell properties and component properties which occur with various heat treatments are now sufficiently well documented that an attempt to compare experimental and theoretical results seems warranted.

For Cu_yS layers on CdS we must take into account the fact that the hole concentration in Cu_yS is probably modified by the presence of a Cd concentration which acts as a donor level and compensates the Cu_yS. Thus we have in Cu_yS

$$p = \{[Cu]_{vac} - 2N_{Cd}\} = 2(10^{22}\, x - N_{Cd})$$

In addition the total density of scatterers is given by

$$N_s = [Cu]_{vac} + N_{Cd} = 2\,(10^{22}x + \frac{N_{Cd}}{2})$$

We can write down a set of equations for sheet resistance, and absorption coefficient in the optical and in the infrared regions, as a function of stoichiometry and compare them with the reported experimental results.

The sheet resistance is given by the relation

$$\frac{\rho}{d} = \frac{1}{dq\mu_p p} = \frac{6.25 \times 10^{18}}{d\ \mu_p\ [[Cu] - 2N_d]}$$

The absorption coefficient of a degenerate indirect gap semiconductor with scattering dominating the momentum conservation relation is given by

$$\alpha\ (h\nu) = A_s N_s\ (h\nu - E_g - E_F')^2$$

where A_s is a coefficient which depends upon the band structure of the material, and E_F' is the energy separation between the valence band edge and the position of the Fermi level (below the valence band). The expression for E_F is

$$E_F' = \tfrac{1}{2}\ (3\pi^2)^{2/3}\ \frac{h^2}{m^*}\ p^{2/3}$$

$$= \frac{3.62 \times 10^{-3}}{(m^*/m_0)}\ \left(\frac{p}{10^{18}}\right)^{2/3}\ \text{eV}$$

The cathodoluminescent signal should have a dependence similar to $\alpha\ (h\nu)$ since it is the inverse process.

The free carrier absorption is given by the relation

$$\alpha_f(\lambda) = cp\lambda^r$$

where c is a factor which depends upon the effective mass of the holes, and r ranges from 1.5 to 3.5 depending upon the dominant scattering mechanism. From Maxwell's equations and Ohm's law a close relation between the free carrier absorption and the resistivity of the material exists i.e.

$$\alpha_f(\lambda) = \frac{\sigma(\lambda)}{\varepsilon_0 cn}$$

where $\sigma(\lambda)$ is the frequency dependent conductivity. With λ in (μm) we can write

$$\alpha_f(\lambda) = \frac{6 \times 10^{-17}\, p\mu}{n} \quad \frac{\lambda^2}{\lambda^2 + 1.15\, \mu^2\, (m^*/m_0)^2}$$

From this expression we see that the variation of μ with stoichiometry will be important in determining both the magnitude and apparent wavelength dependence of the free carrier absorption. Studies of sheet resistance, α optical, and α_f have been reported by Burton and Windawi,[8] and also by Fagen.[9] A quantitative comparison between the theoretical expressions and the experimental data will be reported in the next quarter. Preliminary comparisons indicate that the experimental results can be explained adequately by the equations presented here.

Space Charge Profiles and the Intercept of $1/C^2$ Versus Voltage Plots

In the CdS/Cu_2S solar cell the capacitance in forward bias is usually very unstable. In addition the conductance is often too high for accurate capacitances to be obtained. The reverse bias region is stable, however, and one would like to deduce as much information as possible from this region. Measurements in the dark and with white light or monochromatic light can be carried out. One of the goals of such measurements is to deduce the space charge profile in the CdS layer near the CdS/Cu_2S interface.

A number of models other than the simple uniform space model have been advanced in the past.[11,12] Evidence based on capacitance measurements as a function of heat treatment indicate that a compensated region is established in the CdS (probably due to the diffusion of Cu) and continues to extend into the CdS with longer heat treatments. Both the degree of compensation and the distance into the CdS of the compensation region may change with heat treatment.

In Fig.10 we illustrate various space charge profiles in the CdS layer and the expected $1/C^2$ vs. V. In Fig.10, w (o) is the zero voltage space charge layer width. The diffusion voltage or built-in voltage is given by V_D, the voltage V_I is the intercept of the extrapolated slope at V = 0, with the V axis.

For Fig. 10a the uniform space charge case one has

$$\left(\frac{A}{C}\right)^2 = \frac{2\ (V_D - V)}{q\varepsilon\varepsilon_0 N_D} \tag{5-1}$$

$$\frac{d\ \left(\frac{A}{C^2}\right).}{dV} = \frac{2}{q\varepsilon\varepsilon_0 N_D} \tag{5-2}$$

$$V_I = \frac{\left(\frac{A}{C^2}\right)_{V=0}}{\frac{d\ \left(\frac{A}{C}\right)^2}{dV}_{V=0}} = V_D \tag{5-3}$$

where A is the planar area of the cell. Figure 10b represents the case of a compensated layer of width x_A, with the zero voltage space charge region extending into the uncompensated region. In reverse bias the space charge region will expand into the uncompensated region. As long as the space charge region remains in the N_1 region we can write

$$\left(\frac{A}{C}\right)^2 = \frac{w^2\ (V)}{(\varepsilon\varepsilon_0)^2} \tag{5-4}$$

$$\frac{d\ \left(\frac{A}{C}\right)^2}{dV} = \frac{2}{q\varepsilon\varepsilon_0 N_1} \tag{5-5}$$

$$V_I = \frac{(A/C)^2)V=0}{\frac{d\ (A/C)^2}{dV}_{V=0}} = \frac{w^2\ (o)\ qN_1}{2\varepsilon\varepsilon_0} \tag{5-6}$$

If we had uniform layer of density N_1 the expression for V_D would have been

$$V_D = \frac{qN_1}{2\varepsilon\varepsilon_0}\ w_{N_1}{}^2(o) \tag{5-7}$$

with $$w_{N_1}\ (o) = \left(\frac{2\varepsilon\varepsilon_0 V_D}{qN_1}\right)^{\frac{1}{2}}$$

For a fixed V_D, and by inspection of Fig. 10b, w_{N_1} (o) < w (o) if $N_1 > N_2$. Hence, from Eqs. (5-6) and (5-7)

$$\frac{V_I}{V_D} = \frac{w\ (o)^2}{w_{N_1}{}^2\ (o)} > 1 \qquad (5\text{-}8)$$

The $(A/C)^2$ versus V in Fig.(10b) illustrates this fact.

Fig.10c illustrates a region of higher space charge near the junction, and for x_B a fixed point it is the same as Fig.10b, but with $N_2 > N_1$. Hence as inset (1) shows $V_I < V_D$. There are two variants to Fig. 10c which are of direct interest to the operation of the cell. First if a deep energy level exists in CdS close enough to the conduction band edge to be emptied by the band bending as in Fig. 11, then the position x_B is determined by the crossing of E_F and E_1. This crossing will shift with the bias voltage, moving to the left in forward bias and to the right in reverse bias. Inset (2) of Fig. 10c shows the $(A/C)^2$ vs. V for this case.

A second instance in which Fig. 10c can be established is by the action of light. If we start with Fig. 10a or 10b but with a density of deep acceptor levels E_2 as indicated in Fig. 11 extending into the CdS, then band gap light, or light sufficient to excite electrons from the valence band to an empty state will create holes which can become trapped in E_2 levels, increasing the positive space charge near the interface. This effect causes the marked increase in capacitance seen under illumination in most heat treated cells. For a given illumination intensity and wavelength distribution the steady state situation will produce a constant

x_B situation and give a $(A/C)^2$ vs. V curve similar to inset (1), Fig. 10c. The V = 0 value of C/A can be used in conjunction with the slope of A^2/C^2 vs. V to determine N_3, if the profile in Fig. 10c is caused by only one mechanism.

In Fig. 10d we have the most general case, with the inset showing the expected $(A/C)^2$ vs. V curve.

The sharp changes in the space charge profiles shown in Fig. 10 are likely to be rounded considerably in actual samples as a result of diffusion processes and inhomogeneities in the polycrystalline films. In addition the surfaces of the samples and hence the junctions are not planar. These real sample effects make quantitative comparisons with the models above more difficult. However, the various behaviors indicated in Fig. 10 have been seen in actual cells. Tests on well defined samples are planned.

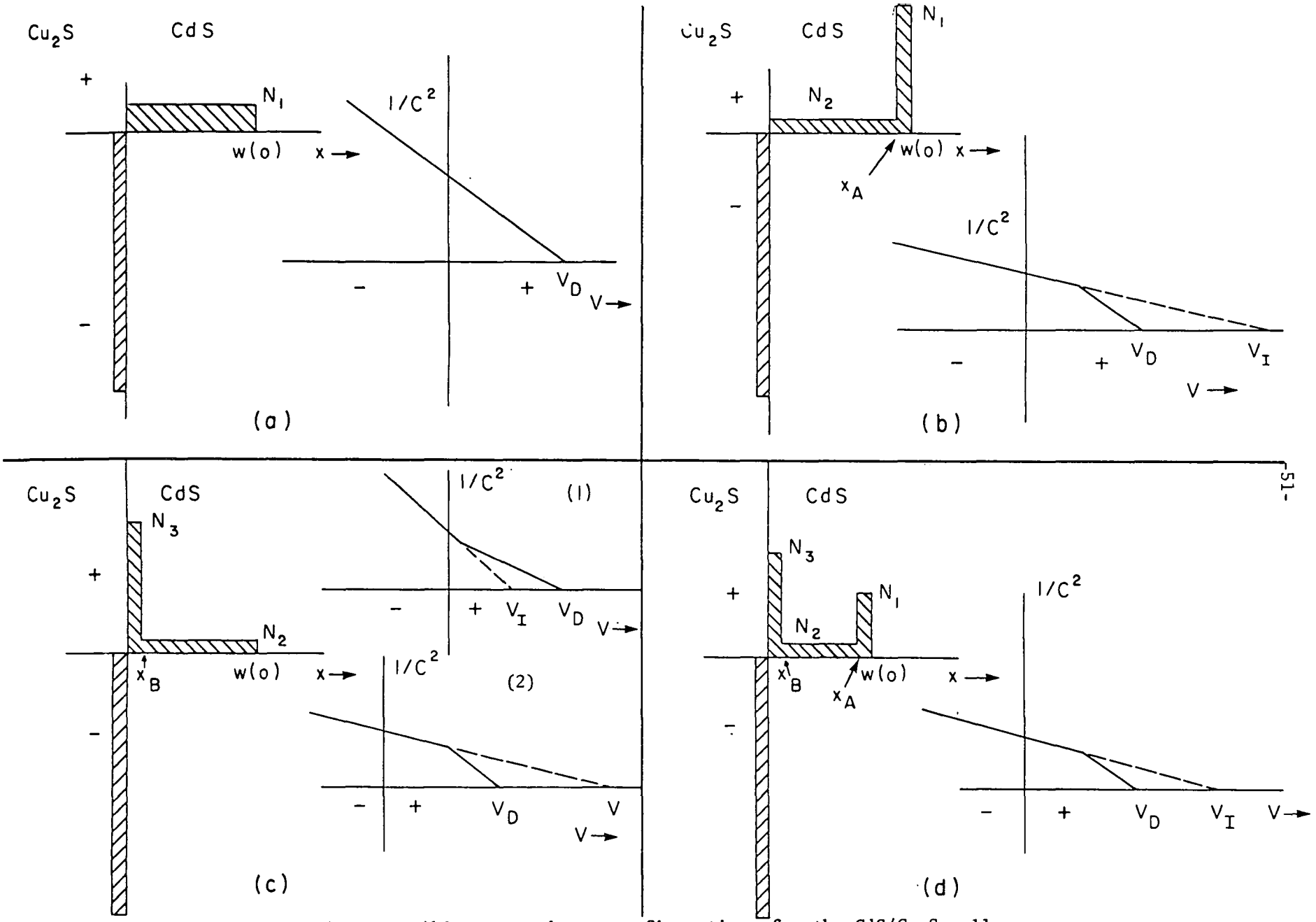

Figure 10. Various possible space charge configurations for the CdS/Cu_2S cell.

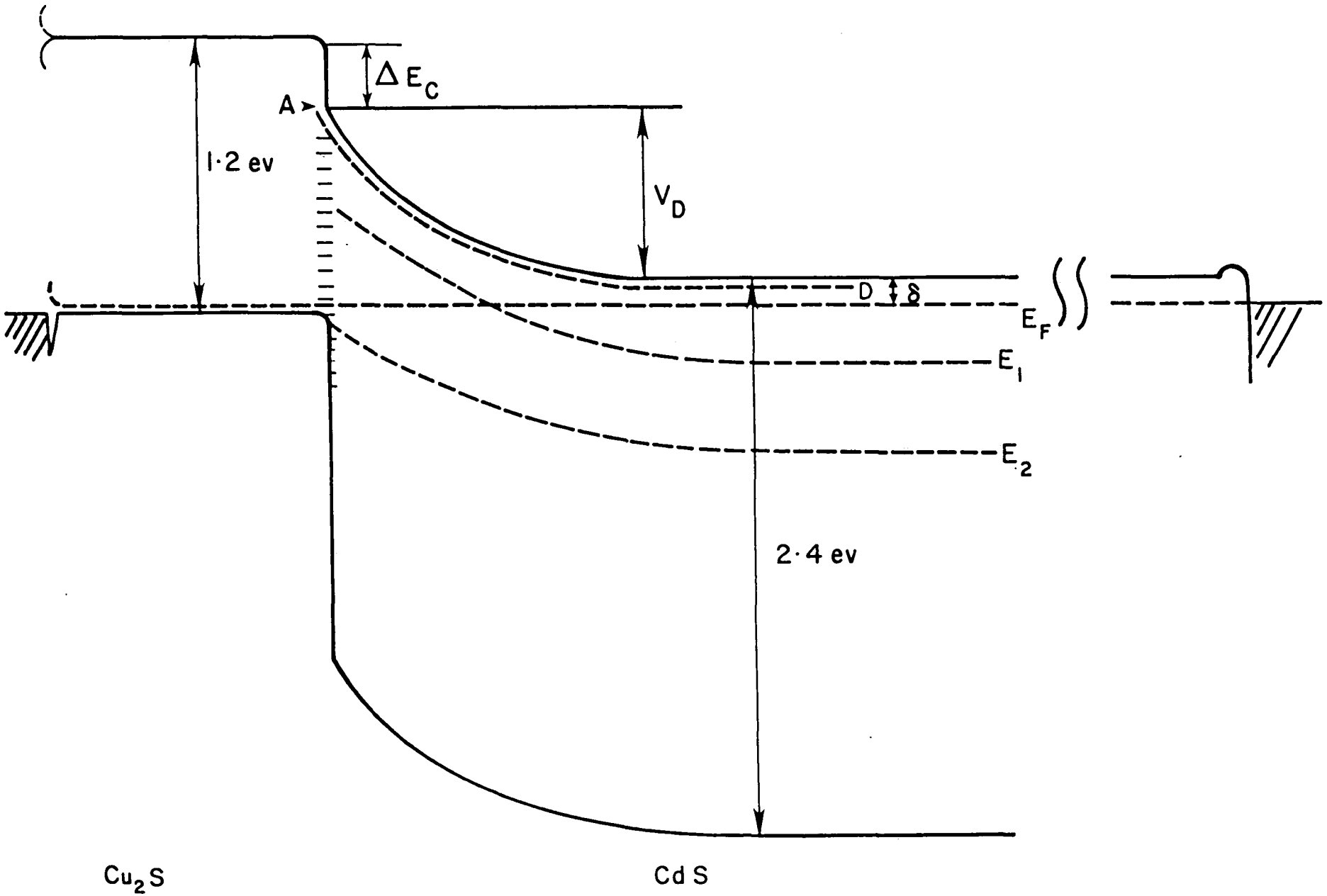

Figure 11. Possible band structures for a CdS/Cu_2S cell.

6. References

1. Progress Report E(49-18)-2538 PR 76/1.

2. T. S. te Velde and J. Dieleman, Philips Res. Repts. 28, 573 (1973).

3. L. C. Burton, B. Baron, W. Devaney, T. L. Hench, S. Lorenz, and J. D. Meakin, Proceedings of the 12th Photovoltaic Specialists Conference, Baton Rouge, La. 1976 (to be published).

4. D. Curie, "Luminescence in Crystals," John Wiley and Sons, Inc., New York (1963).

5. J. Besson, T. Nguyen Duy, A. Gauthier, W. Palz, C. Martin, and J. Vedel, Proceedings of the 11th Photovoltaic Specialists Conference, Scottsdale, Arizona, 1975.

6. G. Z. Idrichan, S. P. Sorokin, Izvestiyer Akademii Nauk SSSR, Neorganicheskie Materialy 11, 1693 (1975) (Eng. Trans. - Inorganic Materials 11, 1449 (1975)).

7. W. Palz, J. Besson, T. Nguyen Duy, J. Vedel Proc. 9th IEEE Photovoltaic Specialists Conference, Silver Spring, Md. 1972, p. 92.

8. L. C. Burton, H. M. Windawi, J. Appl. Phys., 47, 4621 (1976).

9. E. A. Fagen STM-76-3, Institute of Energy Conversion, University of Delaware.

10. J. J. Loferski, J. Schewchun, E. A. DeMeo, R. Arnott, E. E. Crisman, R. Beauliev, H. L. Wang and C. C. Wu, Proceedings 12th Photovoltaic Specialist Conference, Baton Rouge, La., 1976 (to be published).

11. H. W. Brandhorst, Jr., Proc. 7th IEEE Photovoltaic Specialists Conf. 1968, p. 33.

12. Progress Report NSF/RANN/AER72-03478 A03/FR/75, Oct. 1975, Institute of Energy Conversion, University of Delaware, p. 153.

Appendix A

LIST OF RESEARCH CONTRIBUTORS

Dr. John D. Meakin, Associate Director, Principal Investigator

Dr. Allen M. Barnett, Director

Dr. Bill N. Baron, Associate Scientist

Dr. Charles E. Birchenall, Distinguished Professor of Metallurgy

Dr. Larry C. Burton, Scientist

Dr. Walter E. Devaney, Research Associate

Mr. Thomas L. Hench, Research Assistant

Ms. Leslie M. Kilgren, Research Associate

Mr. Steven Lorenz, Electronics Engineer

Mr. George Miller, Senior Laboratory Technician

Dr. Roy L. McCullough, Professor of Chemical Engineering

Mr. Patrick Mulvihill, Graduate Student

Dr. Larry D. Partain, Assistant Professor of Electrical Engineering

Mr. James E. Phillips, Research Associate

Dr. Allen Rothwarf, Senior Scientist

Dr. Joseph Sansregret, Research Associate

Mr. Stephen Shea, Graduate Student

Dr. George Storti, Research Associate

Mr. David Brindle, Instrument Technician

Mr. David Cowgill, Senior Design Machinist

Ms. Gwendolyn A. Howk, Senior Research Technician

Mr. Thomas Lovett, Undergraduate

Ms. Maryanne Powers, Senior Research Technician

Mr. Robert Wieland, Research Technician

Mr. Walter Willing, Undergraduate

Mr. David Potts, Graduate Student

Ms. Sandra Lynn Matthews, Technical Secretary

*U.S. GOVERNMENT PRINTING OFFICE: 1978-740-306/9488. Region 4.